New Journal and we have not received input yet 29 (2022) 101205

Contents lists available at ScienceDirect

Thermal Science and Engineering Progress

journal homepage: www.sciencedirect.com/journal/thermal-science-and-engineering-progress

Numerical heat transfer study of a space environmental testing facility using COMSOL Multiphysics

Abhilash Vakkada Ramachandran [a,*], María-Paz Zorzano [b,c,a], Javier Martín-Torres [a,c,d]

[a] Group of Atmospheric Science, Department of Computer Science, Electrical and Space Engineering, Luleå University of Technology, Luleå 97187 Sweden
[b] Centro de Astrobiología (CSIC-INTA), Torrejón de Ardoz, Madrid 28850, Spain
[c] School of Geosciences, University of Aberdeen, Aberdeen AB24 3FX, UK
[d] Instituto Andaluz de Ciencias de la Tierra (CSIC-UGR), Granada 18100, Spain

ARTICLE INFO

Keywords:
Mars
3D model
Space chamber
Vacuum
Heat transfer
Test facility

ABSTRACT

Environmental chambers are used to test the expected performance of space instrumentation and to investigate certain processes which are relevant in space or other planetary environments. In this study, a computational model of an existing Martian experimental facility is investigated numerically using COMSOL Multiphysics. For this purpose, we simulate the near surface water cycle under Martian temperature and pressure experimental conditions as tested inside the chamber and we compare the simulations with the experimental data. The model shows good agreement with experiments on the equilibration time scales and thermal gradients. Due to the imposibility to place sensors at multiple locations inside the chamber, we use the model to extrapolate the one-point relative humidity of the experimental data to each grid points in the simulation. This model gives an understanding of the gradient in atmospheric water relative humidity to which the experimental samples such as deliquescent salts and Martian regolith simulants are exposed at different time intervals. The of the performance of HABIT instrument during the tests, of the ESA/IKI ExoMars 2022 robotic mission to Mars, when compared with the model shows the existence of an extra internal heating source of about 1 W which can be attributed to the hydration and deliquescence of the salts exposed to Martian conditions when in contact with atmospheric moisture. In addition, the presented model is used to predict the thermal gradients and understand the time response when the chamber is heated in vacuum conditions. Our analysis shows that for thermal vacuum tests, the chamber will take about 2.5 h to reach the test temperature of 420 K.

1. Introduction

The design and testing of instruments, hardware, and materials for space is strongly constrained by the required environmental conditions of operation, namely high vacuum, radiation exposure and varying extreme temperatures. Thus, before launching any spacecraft platform to space, every component or scientific instrument must be tested to demonstrate that it survives through this thermal dynamic process and, when applicable, its functionality must be shown through different thermal ranges within dedicated chambers. Space simulation chambers, capable of reaching high levels of vacuum to simulate the low-pressure environment in deep space, have been developed since the 1960′s, and numerous space simulating facilities have been built for planetary and space research. They have been used for simulating different planetary environments mainly under Martian conditions to test instrumentation and perform research related to its application to astrobiology [1,2,3,4,5]. These chambers are used to perform qualification tests such as Thermal Vacuum Tests (TVT), and outgassing and sterilization through the Dry Heat Microbial reduction (DHMR) tests as defined in the standards [6,7]. These tests have a significant role in validating the integrity and thermal performance of the components.

The boom of space exploration and the potential to demonstrate and investigate *in-situ* Resource Utilization (ISRU) methods for Mars exploration requires developing new instruments that can operate at the surface of such planetary environment. Mars has a very low-density atmosphere with a surface pressure of 6–10 mbar [8] which mainly consists of carbon dioxide (CO_2) gas and traces of water vapor, but the relative humidity (RH) at the surface can vary from 0 % RH to 100 % RH in a single day due to the large diurnal thermal oscillations [9]. The surface temperature can be as low as 142 K [10] on the southern polar caps while the maximum surface temperature can reach up to 300 K

* Corresponding author.
E-mail addresses: abhilash.vakkada-ramachandran@ltu.se (A. Vakkada Ramachandran), zorzanomm@cab.inta-csic.es (M.-P. Zorzano).

https://doi.org/10.1016/j.tsep.2022.101205
Received 26 May 2021; Received in revised form 22 November 2021; Accepted 12 January 2022
Available online 15 January 2022

Nomenclature

C_p	Heat capacity at constant pressure [J/(kg*K)]
D_{gas}	Kinetic diameter of the gas considered (m)
$ew_{liq(T)}$	Saturation partial pressure over liquid water at given temperature
$ew_{ice(T)}$	Saturation partial pressure over ice at given temperature
F	Volume force field [N/m^3]
k	Thermal conductivity [W/(m*K)]
k_B	Boltzmann constant
L_c	Characteristic length
P	Fluid pressure (mbar)
Q	Heat source [W/m^3]
q	Heat flux [W/m^2]
RH	Relative humidity (%)
RH_a	Air relative humidity (%)
RH_g	Ground relative humidity (%)
T	Temperature [K]
T_a	Air temperature [K]
T_{ext}	External temperature [K]
T_g	Ground temperature [K]
u	Velocity field [m/s]
vmr	Volume Mixing Ratio in parts per million (ppm)
W	Water mass mixing ratio
ε	Emissivity
μ	Fluid dynamic viscosity (Pa.s)
λ	Mean free path between the gas molecules
σ	Stefan–Boltzmann constant

[11]. Simulating these representative conditions in the laboratory environment gives us a better means to evaluate the responses of the scientific payloads which can provide us a valuable support while interpreting the mission data and planning the operation of instruments. But considering the spatial constraints in the simulation chambers to mount sensors at multiple locations is not a feasible idea. Hence most of the chambers rely on one-or two-point measurements from the sensors to interpret the data of the entire system.

Previous works have documented similar simulation studies for various facilities, and where possible, certain measured variables are compared with the simulations. For instance, recently a simulation based on FLUENT software has been implemented and validated at a pressure of 1500 Pa, (15 mbar) to predesign a potential future wind facility box operating under Martian pressures. The preliminary results have been presented in the form of conference proceedings [12]. In another work, numerically solved finite element technique written using the Buongiorno's nano liquid approach of a cubical cavity containing a cylinder and a heat source is studied for the convective energy transport within the chamber saturated by nanofluids by comparing the 2D and 3D analysis with the experimental data [13]. The foreseen fluid flow and heat transfer characteristics for horizontal and vertical CO_2 enclosures on the surface of Mars have been investigated by numerical studies using FLUENT 14.0 software [14]. A Monte Carlo 3D simulation has been done to study the radiative heat exchange inside vacuum furnaces [15]. A conjugate heat transfer study using FLUENT has been used to predict the transient temperature fields of a rocket combustion chamber and has been compared with the experimental results [16]. Several finite element method (FEM) software's such as COMSOL Multiphysics, ANSYS FLUENT and other packages have been used to study the heat transfer characteristics of different instruments for mass gauging, validation with experimental results for testing facilities and for other purposes [17,18,19,20,21,22,23,24,25]. COMSOL has also been used to simulate, the thermal environment in large rooms with specific thermal insulation and heat transfer for different external conditions [26].

In this work we use the SpaceQ facility, which was developed at the Luleå University of Technology, Sweden, to test the performance of hardware and certain products under vacuum and Martian conditions [27]. We implement and validate a heat-transfer simulation to investigate the thermal behavior and provide insight into the expected relative humidity within the chamber under different operating scenarios, see Fig. 1. The SpaceQ chamber operates in the pressure range from $<10^{-5}$ mbar (high vacuum) to ambient pressure and in a temperature range from 163 K to 423 K. It is mainly used to mimic the plausible near surface Martian water cycle by injecting minute amounts of water

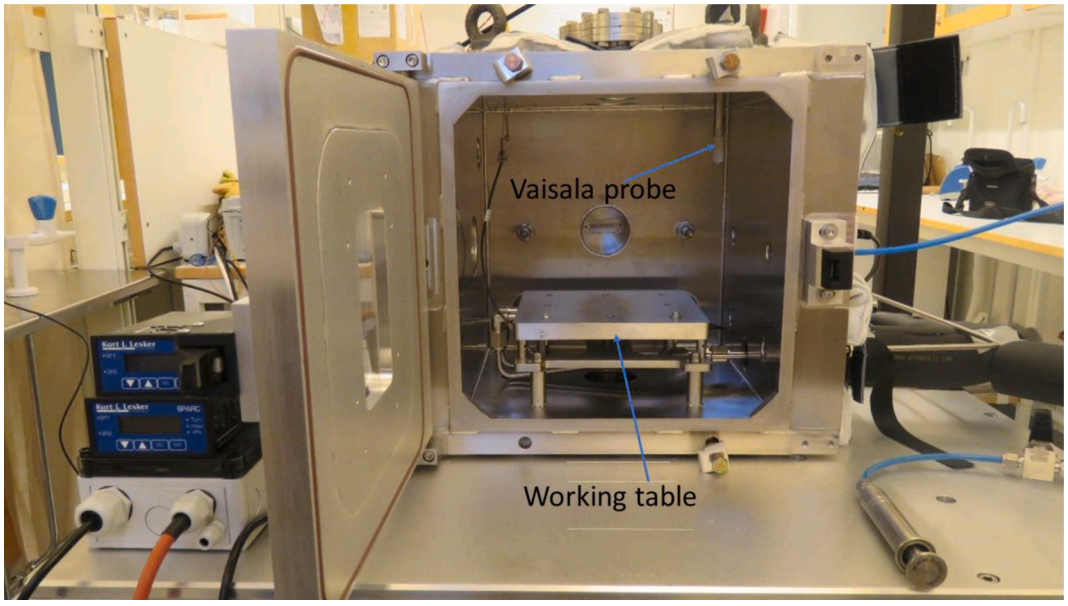

Fig. 1. Internal view of the SpaceQ chamber, a 300×300×300 mm^3 cubical chamber, with its volume of 27 l, showing the working table (200 mm squared plate with a thickness of 18 mm) used to refrigerate and the Vaisala Relative Humidity probe used to measure temperature and relative humidity of the air.

through a syringe into the chamber. The temperature of the chamber is controlled by two means: (i) cooling of the chamber is performed by passing liquid nitrogen through the working plate with a proportional integral derivative (PID) controller which is in feedback through a temperature sensor; and (ii) heating is performed by an external jacket wrapped on the chamber walls that can operate from ambient temperatures up to 423 K. The SpaceQ has been mainly designed for (i) simulating Martian conditions and (ii) to test and qualify instrumentation and materials for space with varying thermal, water content and/or pressure changes. The chamber can also be used to qualify components for space operations by performing TVT, outgassing, and sterilization through DHMR tests.

This paper introduces and validates a computational model to investigate the transient temperature field of this test facility. Here we have used the COMSOL Multiphysics Heat transfer module's Conjugate Heat Transfer Laminar Flow model to solve the heat-flux and the Navier-Stokes equations under certain given boundary conditions and compare the simulation temperature control points with temperature sensors from experiments to understand the equilibration time scales and thermal gradients. The computational results will then be used to increase our understanding of the existing thermal gradients in our laboratory facility and to understand the implications and limitations for the practical applications of the chamber for tests and experiments. For example, one of the cases where thermal gradients may affect the experiments is when water is incorporated as a minor component of the atmospheric composition. As the SpaceQ chamber is subjected to a temperature difference produced either by cooling or heating locally, while being immersed in a laboratory environment at room temperature, a thermal gradient will inevitably be developed. And this will influence the local relative humidity (RH), which is strongly dependent on temperature. The existing, unavoidable, temperature gradients may thus have an influence on the planning and interpretation of the experiments. Water may condense where the temperature is very low and there is saturation, while it may be in gaseous phase elsewhere. Since in the SpaceQ chamber the relative humidity (RH %) is only monitored at one point with a dedicated probe, its extrapolation to the rest of the chamber using the model must be inferred through the local temperature (T) and pressure (P) field. Pressure equilibrates within the full chamber, and thus a single point measurement is sufficient. However, the temperature can be only measured at a few spots within the chamber due to the natural room limitations of this closed facility. Computer thermal simulations can be used to extrapolate this field to other points.

This work is, to our knowledge, the first report devoted to simulating an existing Martian environment experimental facility. The heat transfer simulation study may serve for the space and engineering community, to be applied in their own facilities in the previous phases of designing chambers and experiments. Without loss of generality, we will illustrate the usefulness of this kind of simulations with a few specific applications for the SpaceQ chamber facility.

2. Materials and methods

2.1. Summary of the SpaceQ chamber facility

To simulate the space and Mars environment for different research and technological applications, the SpaceQ chamber (Fig. 1) has been developed [27 28]. It can cover a range of environmental conditions, from ambient pressures to $<10^{-5}$ mbar and temperatures between 163 K and 423 K which are reached by cooling the working plate with liquid nitrogen or heating the walls with an external heating jacket. We use a Vaisala HMT 334 sensor to measure the ambient air temperature and relative humidity at one spot of the chamber. This sensor can measure the temperature in the range of 203.15 K to 453.15 K with an accuracy of ± 2 K and the relative humidity from 0 to 100% RH with an accuracy of ± 1% RH. A KD Scientific stainless-steel syringe with a capacity of 20 ml from Fischer Scientific fitted on to a ¼'' Swagelok connector is used to inject water into the chamber. It has several utility ports including two view ports (Zero-Length,4–1/2″ UHV), thermocouple feedthroughs, pressure control Pirani gauge (range of 1×10^{-9} mbar to 1000 mbar), gas inlets, rotary and molecular turbo pump ports, USB connections, and DB25 to read the instrumentation data in real time.

A Martian atmosphere is created by vacuuming the chamber to 10^{-3} mbar and then 100% pure CO_2 gas is injected from a cylinder until the pressure inside the chamber reaches 7 mbar (average pressure range on Mars). Trace amounts of water are injected into the chamber through a stainless-steel syringe. Then liquid nitrogen (LN_2) is used to refrigerate the working plate that acts as ground surface. For some experimental conditions, saturation is reached at the cooling table. When liquid nitrogen is turned off the temperature raises by equilibration with the external laboratory conditions. If frost has been formed, as the temperature of this plate increases slowly, water is released slowly back to the atmosphere, thereby producing a near surface water cycle.

Under vacuum conditions (i.e., without CO_2 or water injection), this chamber can also be used to perform Thermal Vacuum Test (TVT) (ECSS-Q-ST-70-02C), outgassing, and sterilization through dry heat microbial reduction (DMHR) tests (ECSS-Q-ST-70-57C).

2.2. Governing equations, boundary conditions and COMSOL implementation

To simulate the system, we assume the fluid flow to be continuous inside the chamber with Knudsen number $K_n = \lambda/L_c < 0.1$, where λ is the mean free path between the gas molecules and L_c is the characteristic length [29 30 31]. The average number of mean free path gas molecules inside the chamber is calculated with the equation 1

$$\boldsymbol{\lambda} = \frac{\boldsymbol{k_B T}}{\sqrt{2}\boldsymbol{D_{gas}^2 P}} \tag{1}$$

where, $\boldsymbol{k_B}$ is the Boltzmann constant,

T is the air temperature,

P is the air pressure,

D_{gas} is the kinetic diameter of the gas considered.

The kinetic diameter $\boldsymbol{D_{Co2}}$ is assumed to be 3.9×10^{-10} m according to [32]. The average mean free path of the CO_2 molecules inside the chamber according to the calculation is found to be 8.3144×10^{-6} m for the air temperature of 285 K and air pressure of 7 mbar. So, the Knudsen number is of the range 1.662×10^{-4}, this shows the fluid flow inside the chamber is continuous and hence the Navier-Stokes equation is applicable for this study. We consider laminar flow because in low vacuum conditions during the experiments the gas particles are assumed to be in the layers constantly parallel to each other, this might change into turbulent flow only when the pressure is manipulated during the gas pump down processes (or venting). So, for simplicity, in this model of the SpaceQ chamber we use COMSOL's conjugate heat transfers laminar flow model.

The geometry of the chamber is shown in Fig. 2, which shows a wireframe of the model dimension $300\times300\times300$ mm^3 cubical chamber fitted with the working plate of dimensions $200\times200\times18$ mm^3 and an external heating jacket. When we simulate Mars conditions, we disabled the heating jacket option (which is only used for thermal heating tests under vacuum conditions). The simulating materials are taken from the in-built COMSOL library, as shown in Table 1. This library takes into account the changes of properties with respect to temperature. The external walls of the chamber are stainless steel, the working plate is aluminum, the heating jacket is made of glass wool and the internal gas is CO_2 for Martian and air for vacuum simulations. To compare the temperature profile with the experimental results, the temperature is monitored at two control points: at 162 mm above the working table and on the working table, see Fig. 2c.

In this study, we use time dependent heat transfer equation (2) and the Navier-Stokes equations for the motion of fluids in the case of

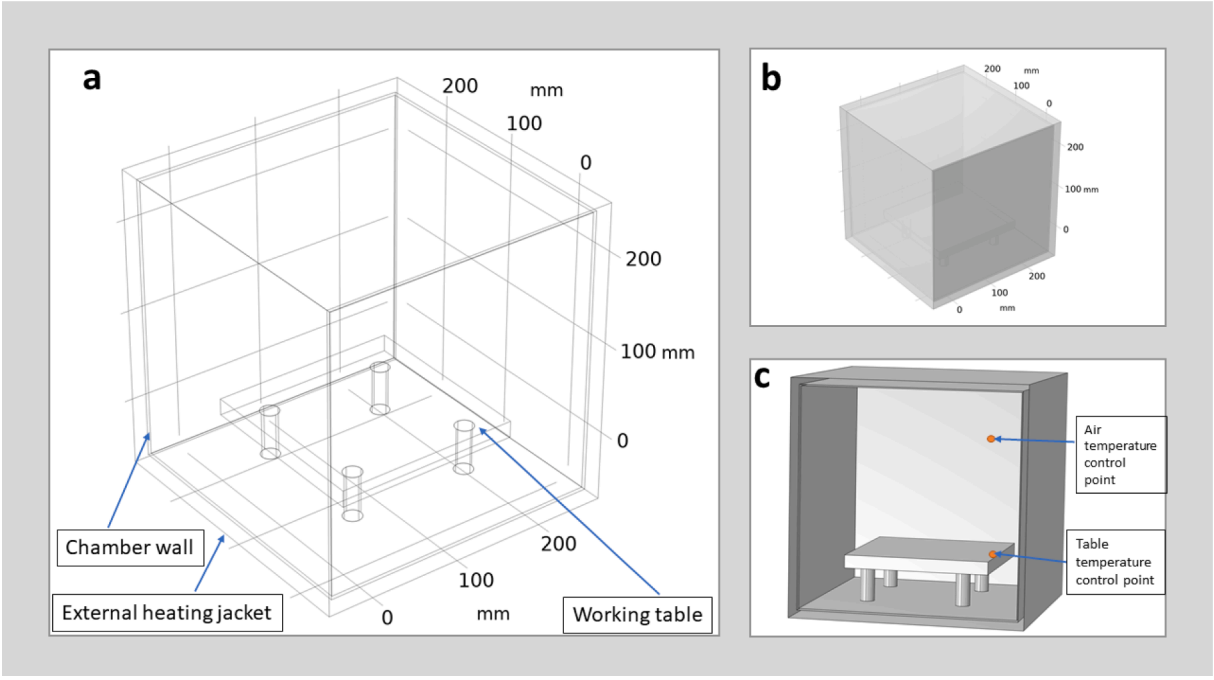

Fig. 2. Geometrical model of the SpaceQ chamber built in COMSOL (a) wire frame model showing the working table and the external wall of the chamber covered with a heating jacket and the point probe for air temperature measurements (b) overview of the 3D model of the chamber (c) 3D model of the chamber with the front boundary disabled showing the temperature monitoring probes.

Table 1
Model parameters value used in the COMSOL simulations.

Parameters	Value	Unit
Conditions for Mars simulations		
Pressure of CO_2 gas	7	[mbar]
Initial CO_2 air temperature	285	[K]
Ambient external temperature	295.15	[K]
Conditions for Vacuum simulations		
Pressure of air	10^{-3}	[mbar]
Initial air temperature	293.15	[K]
Ambient external temperature	295.15	[K]
Aluminum		
Density	2700	[kg/m^3]
Emissivity	0.07	
Thermal conductivity	238	[W/(m*K)]
Heat capacity at constant pressure	900	[J/(kg*K)]
Stainless Steel		
Density	7850	[kg/m^3]
Emissivity	0.6	
Thermal conductivity	44.5	[W/(m*K)]
Heat capacity at constant pressure	475	[J/(kg*K)]
Acrylonitrile butadiene styrene (ABS)		
Density	1050	[kg/m^3]
Thermal conductivity	0.13	[W/(m*K)]
Heat capacity at constant pressure	1400	[J/(kg*K)]
Glass wool batt		
Density	22	[kg/m^3]
Heat capacity at constant pressure	850	[J/(kg*K)]

compressible Newtonian flow to study the fluid density in response to pressure change (3) solved together with the continuity equation (4). The equations that describe this system are

$$\rho C_p \frac{\partial T}{\partial t} + \rho C_p u.\nabla T = \nabla.(k\nabla T) + Q \tag{2}$$

$$\rho\left(\frac{\partial u}{\partial t} + u.\nabla u\right) = -\nabla p. + \nabla.(\mu(\nabla u + (\nabla u)^T) - \frac{2}{3}\mu(\nabla.u)I) + F \tag{3}$$

$$\frac{\partial \rho}{\partial t} + \nabla.(\rho u) = 0 \tag{4}$$

where,
ρ is the fluid density [kg/m^3],
C_p is the heat capacity at constant pressure [J/(kg*K)],
T is the temperature [K],
u is the velocity field [m/s],
k is the thermal conductivity [W/(m*K)]
Q is the heat source [W/m^3],
u is the fluid velocity field [m/s],
p is the fluid pressure [Pa],
μ is the fluid dynamic viscosity [Pa.s],
F is the volume force field [N/m^3],

Heat flux through external natural convection is applied on (i) the 4 vertical walls, with a length of 304 mm, and (ii) the upside horizontal plate, with a characteristic length of 304 mm, of the chamber. This is represented by Robin's boundary condition as in equation (5)

$$q = h(T_{ext} - T) \tag{5}$$

Here, in this study, the heat flux through the bottom surface is neglected as this bottom external surface is attached to a steel frame on which the entire chamber is mounted. We have not included the frame which supports the chamber in this version of the model, but this will be implement in the future study.

where, q is the inward heat flux [W/m^2],
h is the heat transfer coefficient
T_{ext} is the external temperature [K],
T is the temperature at the boundary [K].

The surface-to-surface radiation condition is applied to all boundaries to account for the shading and reflection between radiating surfaces as represented in equation (6)

$$q = \epsilon\sigma(T^4 - T_{amb}^4) \quad (6)$$

where,

q is the heat flux [W/m^2],

ε is the emissivity,

σ is the Stefan–Boltzmann constant

T is the temperature of the boundary [K],

T_{amb} is the ambient temperature [K].

The external boundary was considered at room temperature of 295 K and the working table that is used to simulate Martian surface temperatures was refrigerated to 200–250 K, which is a typical Martian surface night-time temperature, with pressure in the fluid domain at 7 mbar of CO_2. Notice, that for simplicity, for the experiments with minor amounts of water (8 ml) we disregard the thermal properties of water in the atmosphere and the phase state changes under Martian conditions, i.e., we assume a pure CO_2 atmosphere. For the simulation studies presented in section 3.2 with HABIT instrument configuration we shall use similar conditions as mentioned above to simulate Martian temperatures and pressure, adding to the simulation in this case only the heater that is fitted to the instrument. The initial temperature of the HABIT instrument is set initially at 243 K and the simulated heater activates as the temperature goes below 240 K. This simulation is done to understand the energy dissipation when heaters are activated and to quantify the effect of salts hydration in the thermal equilibration of the system. For the studies under vacuum conditions, presented in section 3.3, we consider the external domain as the heat source with 700 W power and the fluid domain inside the chamber as air with a pressure of 10^{-3} mbar and the temperature as ambient initially.

2.3. Simulation setup

A simplified 3D model of the chamber was built to reduce the number of elements and avoid possible errors during meshing. So, all the flanges, nuts and bolts were not modelled. The model was setup in COMSOL Multiphysics 5.6 on a computer with 64-bit operating system, Intel® Core ™ i7-7700 CPU 3.6 GHz processor and 16 GB RAM.

A model with a good mesh should aim for high element quality (>0.01), sufficient resolution and low computational cost but each of these factors are codependent. Keeping these factors in mind we have modelled a 3D coarser mesh (Fig. 3) with 112,185 tetrahedra, 754 pyramids, 20,866 prisms with others a total of 133,805 elements where each of the elements are measured by a skewness quality with a minimum element quality of 0.01059 and an average element quality of 0.5691. The initial model for 3D was done with two types of mesh to compare the results as shown in Table 2. The extra coarse mesh had a total of 63,693 elements and a minimum element quality of 0.008234, this is considered as a low quality hence a coarser mesh was implemented to obtain a better result. Finally, another coarse mesh with 313,779 elements and minimum element quality of 0.01684 was also generated. This later mesh requires too long computational times, and it was not practical for simulations in standard personal computers. The comparison of the result of the different meshes, to obtain the temperature at 7 mbar pressure under Martian conditions at two control points, shows a small variation: the coarser mesh with a maximum error value of 3.72% had an overall average percentage difference of 0.05% when compared with the experimental measurement of the table temperature (Tg) for one specific experimental setup under representative Martian conditions, see Fig. 4. As we shall see, the main temperature error sources are not attributable to the computational mesh but to the simplified simulation setup where certain elements, like the nitrogen pipe whose influence dominates at the beginning of the experiment, are not included. We conclude that beyond this level of resolution the model produces similar results, and therefore we use the coarser mesh model which, given all the uncertainty sources in our model, is sufficiently good for our studies.

The time step used in our studies is automatically selected using the implicit backward differentiation formula (BDF) time stepping method because of its accuracy to provide tolerances at low computational cost and maximum robustness. This solver uses backward differentiation formula with a variable discretization order and selects the step size automatically. These step sizes are adapted based on the local error estimates in relation to the tolerances and the solution of the output times are computed by interpolation between the steps taken by the solver.

Table 2
Comparison of different mesh parameters.

Mesh	Number of elements	Minimum element quality	Computational time required for 400 min of simulation
Extra coarse	63,693	0.008234	47 min
Coarser	133,805	0.01059	4 h

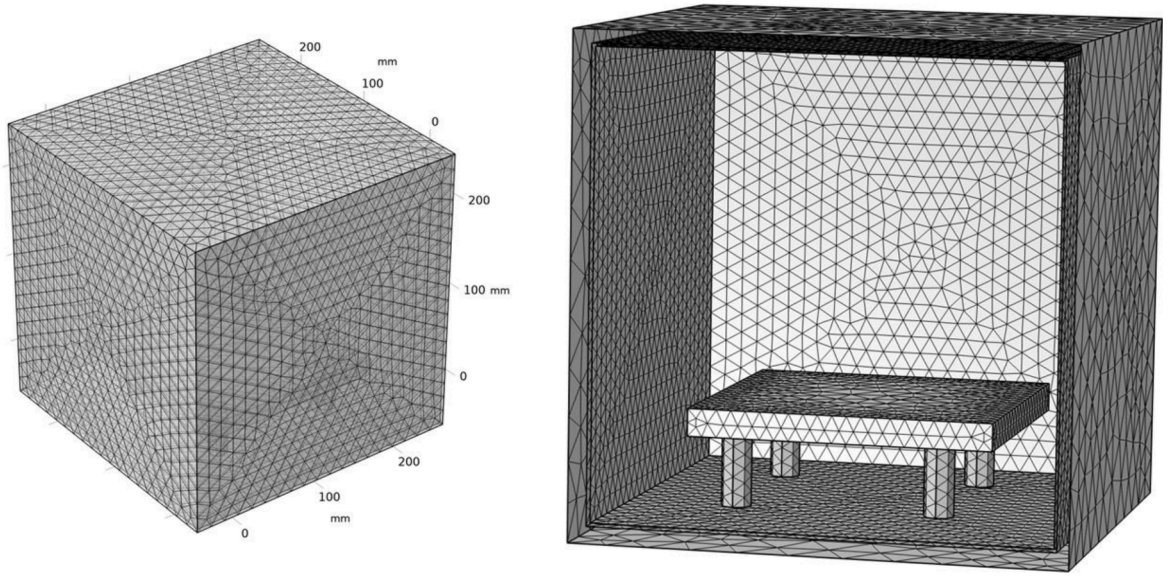

Fig. 3. Meshed model (left) sketch of the 3D coarser mesh (right) inside view of the meshed chamber model.

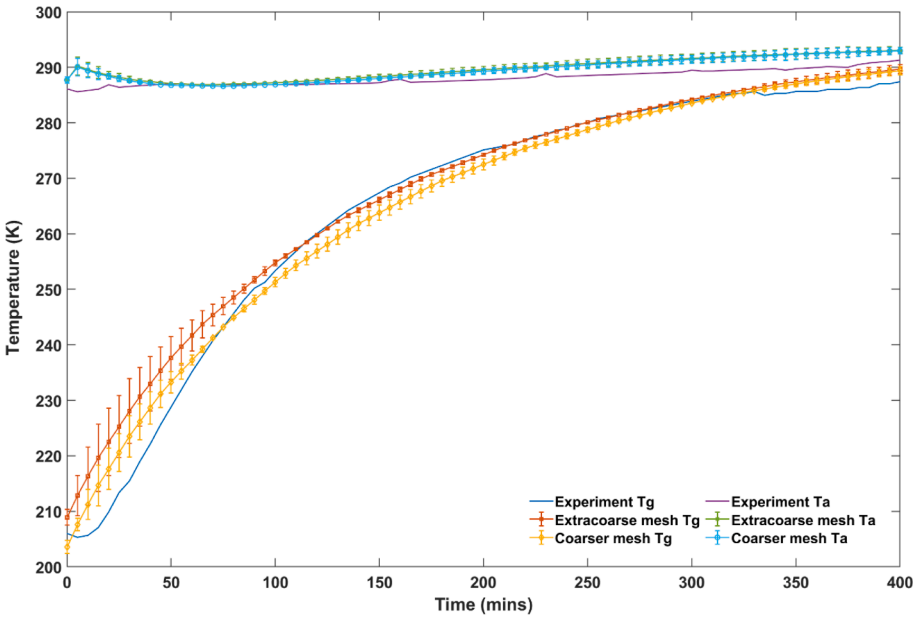

Fig. 4. Comparison of the evolution of the experimental and simulated temperature profile under Martian conditions at 7 mbar pressure for different mesh types, compared for the table temperature (Tg) and air temperature (Ta). This experiment is further described in Figs. 5 and 6.

3. Results and discussion

3.1. Near surface Mars conditions

3.1.1. Dry simulations

The time evolution of the temperature and heat transfer inside the chamber filled with 7 mbar CO_2 gas were investigated. We take two thermal control points, one on the working table and the other 162 mm above the working table, to compare with the experimental data of "ground" temperature (Tg) and air temperature (Ta). The time dependent evolution of the system is investigated for a period of 400 min (6.7 h), as this is the time taken in the experiment to equilibrate with the ambient temperature once the liquid nitrogen cooling of the table has been switched off. The total time taken for the 3D model to compute the results is approximately 3 h. The temperature evolution comparison in 3D and a 2D cross-section is shown in Fig. 5 at different time intervals of 0, 200 and 400 min. At the start of the simulation the working plate is set to 250 K. As the system is allowed to evolve the temperature increases slowly to 290 K due to the contact with the ambient laboratory environment.

Fig. 6 shows the time evolution of the temperature profile of this simulation, at the two thermal control points, and the temperatures

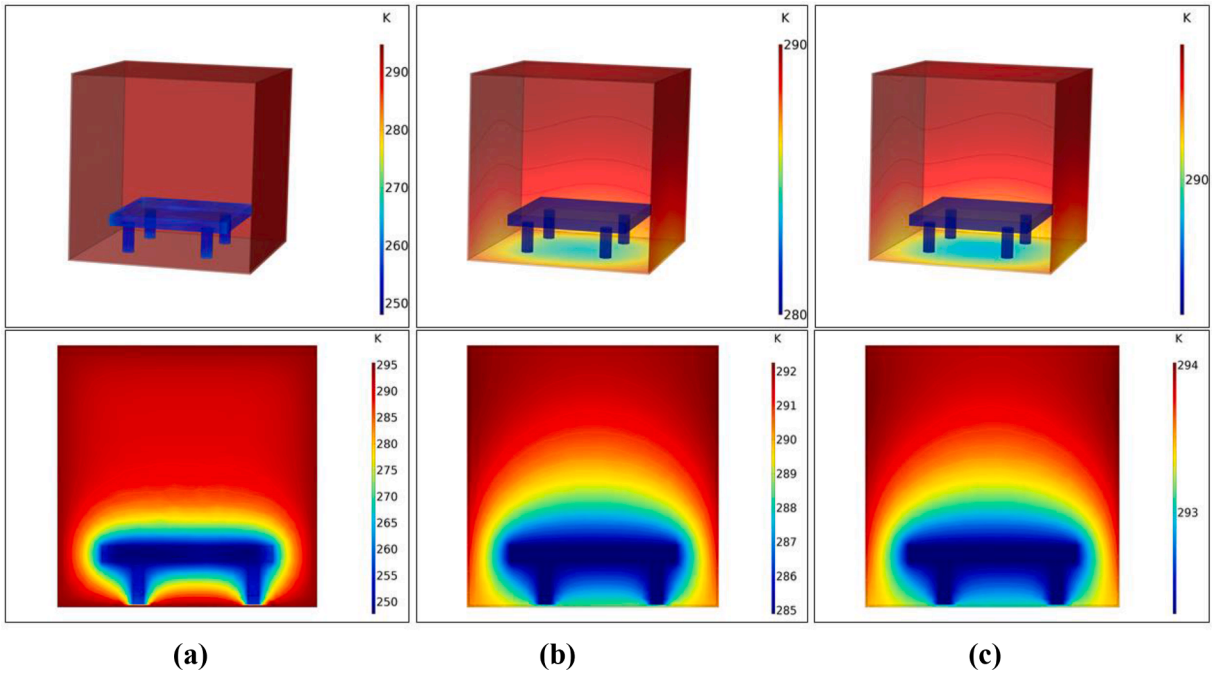

Fig. 5. Time evolution of the temperature inside the chamber (Top) 3D model of the chamber (Bottom) 2D cross section view model of the chamber (a) shows the overview of the temperature distribution inside the chamber at 0 min with the working plate close to 250 K (b) temperature at 200 min (c) at 400 min, almost reaching ambient temperature conditions.

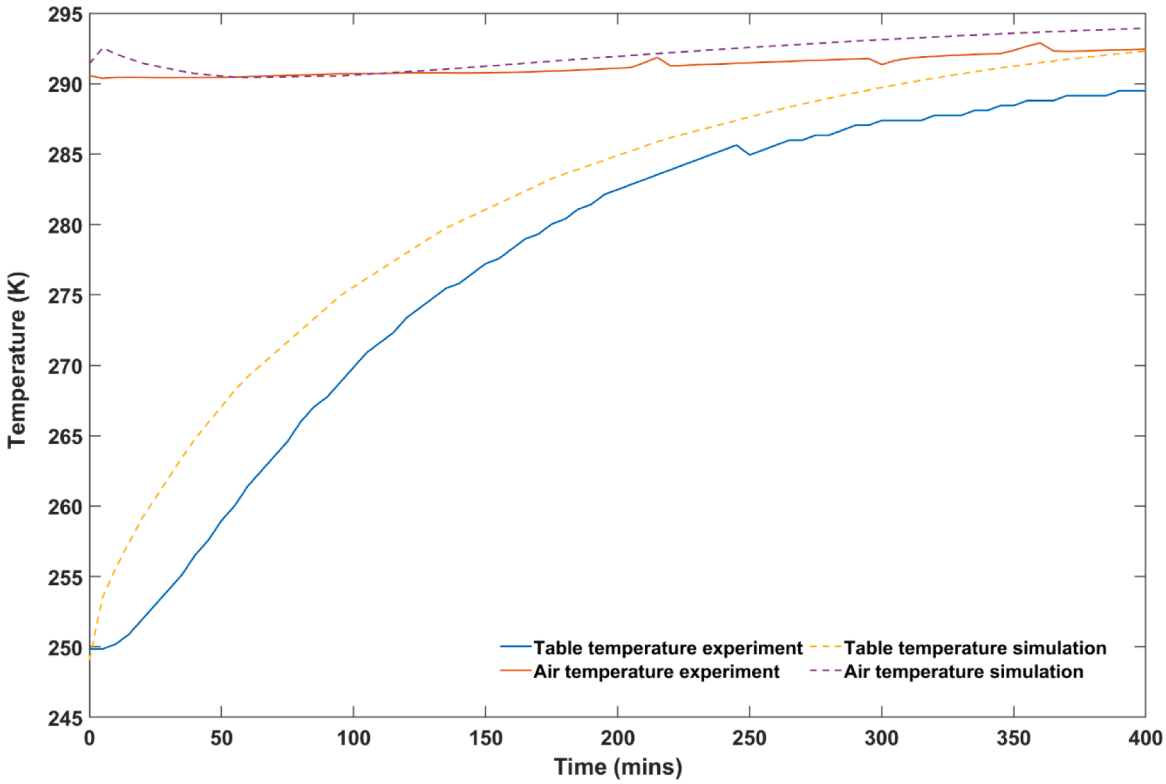

Fig. 6. Comparison of the time evolution of the table temperature (Tg) and air temperature (Ta) under Martian conditions at 7 mbar from COMSOL simulation and experimental measurements.

measured in the experiment. The ground/working table temperature (Tg) and the air temperature (Ta) of both simulation and the experiment follow a similar trend. We observe how the temperature of the working table increases over time from 250 K to 290 K until it reaches equilibrium. The observed differences are attributed to parts that have been omitted in the simulation. For instance, at the beginning, there is some discrepancy between the temperature of the simulation and the measurements, probably due to the thermal inertia of the liquid nitrogen pipe which is not simulated in the model. This shows that the COMSOL simulation that has been designed can be used to plan different experimental setups and estimate thermal gradients and thermal equilibration times.

3.1.2. Water cycle simulation:

In this study, we validate the simulation results with the experimental data during an experiment that simulates the near surface water cycle of Mars. In the experiment [33], we consider the working table as a Martian ground assuming no regolith (a layer of dust, soil or broken rock) or salts exists, simulating a non-porous Martian bedrock. We consider a Martian environment condition to simulate a plausible night-day transition where the initial surface temperature is minimum while the air above is warmer. The experiment is started by evacuating the chamber with a rotary pump to a pressure of 10^{-3} mbar and is filled with pure CO_2 gas till the pressure reads 7 mbar. Next using a stainless-steel syringe, we inject 0.5 ml of water into the chamber in multiple steps while the relative humidity of the air is monitored. Then, the liquid nitrogen is passed through the pipes to refrigerate the working table which acts as a cold sink simulating the Martian surface. As the temperature cools down from ambient to 250 K the water vapor in the air condenses rapidly on the table by reducing the atmospheric water mass mixing ratio and in turn the atmospheric relative humidity, once we observe the frost formation on the table then the LN_2 supply is switched off. During the experiment, the air and surface relative humidity were significantly different due to the thermal gradient between the air and the ground. For this amount of water and this range of temperatures, as we shall see, at the table, saturation conditions are met for ice and liquid water formation. As the temperature of this plate increases slowly, the water was later released slowly back to the atmosphere, allowing for the air relative humidity to increase again. This is how we have simulated the plausible near surface water cycle during the night-day transition on Mars. Here, in this heat transfer study we simulate the temperature and pressure conditions similar to that of the experiment except that, for simplicity, we do not include the small amounts of water vapor in the fluid parameters. Instead, we use the one-point measurement of relative humidity from the experimental data (RHa), and we derive its value for each grid point of the rest of the chamber using the obtained temperature and pressure values from the simulation. This helps us understanding the relative humidity distribution inside the chamber. We calculate the relative humidity using equations 6–10 [9], see Fig. 7. In this experiment, we injected a total of 8 ml of water, maintaining the P between 7 and 8 mbar. In our simulations, however, we keep a constant pressure of CO_2 of 7 mbar, and we ignore water phase state changes. Also, we have not included the water vapor condensation and sublimation, which should also contribute to the heat-transfer problem. Our results indicate that water should first condense on the refrigerated table, at 250 K, where the relative humidity is saturated, and frost should form. As the temperature increases to 290 K or computational simulation shows that water will be redistributed and at the end the full chamber will be almost saturated, see Fig. 7. For instance, in this configuration the atmospheric relative humidity is below 80% beyond 40 mm at 200 min and falls below 80% beyond 50 mm at 400 min above the refrigerated table. This shows that at the end, at ambient temperature the water has been released from the table and the full chamber is almost saturated. Our experimental observations confirm this trend. Fig. 8 shows the time evolution of the relative humidity of the working table in the simulation model shows saturation as expected at the beginning, as the table is refrigerated at 250 K and covered with frost in the experiment. This frost disappears as temperature increases and

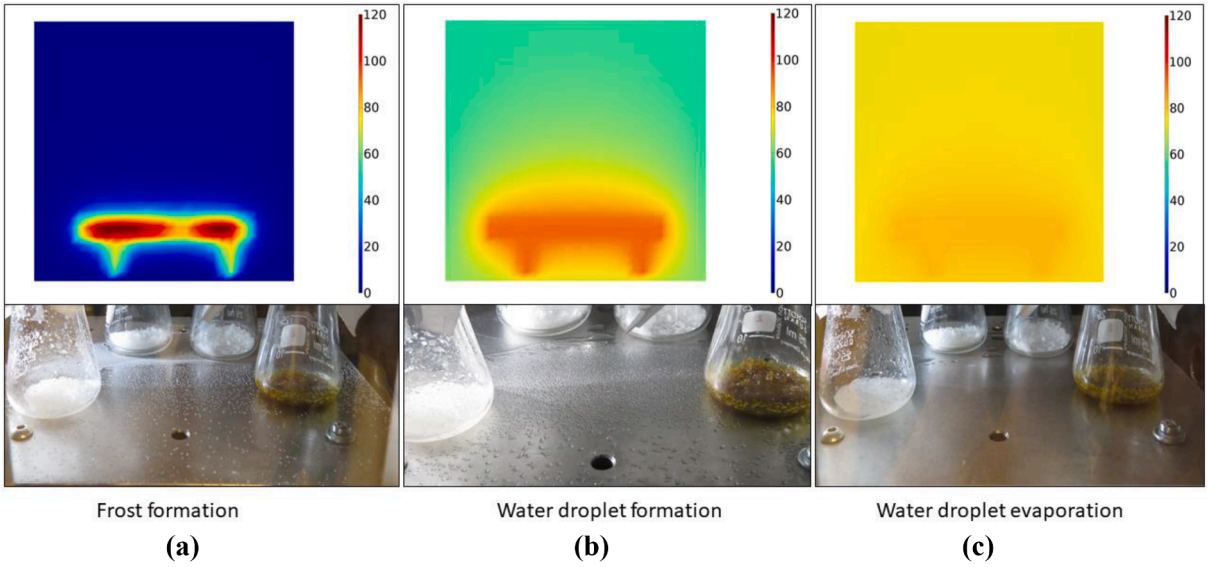

Fig. 7. (Above) 2D cross-section of the time evolution of the relative humidity RH inside the chamber in percentage (%). The atmosphere is saturated for values above 100 % (Below) Images of the water on the refrigerated table of the chamber during the experiments, at the corresponding time. (a) shows the overview of the relative humidity inside the chamber at 0 min when there is over saturation at the working table which for these conditions shall lead to frost formation (b) RH at 200 min, at this RH frost is no longer stable and should sublimate or be transiently stable as liquid, (c) RH at 400 min, at this time the table-condensed water has completely been released to the ambient.

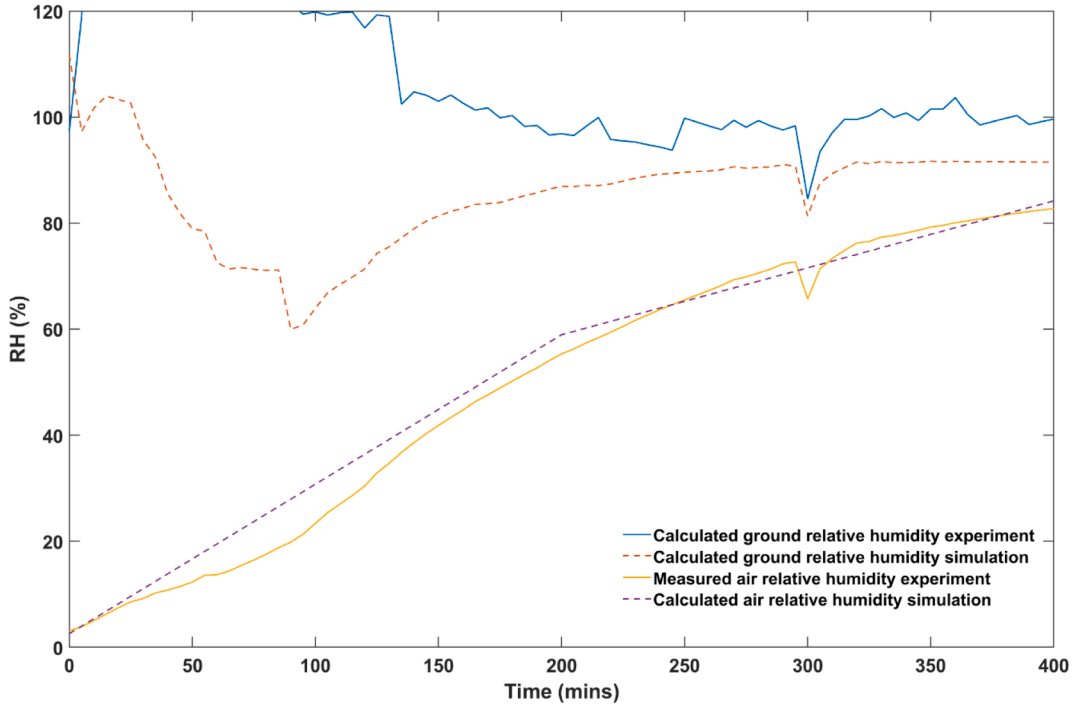

Fig. 8. Calculated relative humidity of the ground (RHg) from the simulation and the experiment showing over saturation (>100%) at the start due to frost formation. This slowly converges towards 100% as water droplets form on the table. While water sublimates and evaporates from the table, the relative humidity of the air (RHa) increases.

water is released to the atmosphere. Through some transient time, a few droplets of water are formed on the surface. Notice that the working table is made of aluminum and is hydrophilic with droplet contact angle <90°. To derive the relative humidity of a given point inside the chamber we use the 31,647 random generated exported data points for different grid point temperature (T), one point air temperature (Ta) at the spot where the RH probe is measuring, pressure (P) values from the simulation which is constant at 7 mbar throughout the simulation. Then we use the measured relative humidity of air (RHa) from the experiment at one point to calculate the overall relative humidity (RH). Fig. 8 shows how this is applied to calculate the relative humidity at the table RH (Tg).

$$\mathrm{RH(T)} = \frac{\mathrm{P}}{\mathrm{ew}_{(\mathrm{T})}} \times \frac{\mathrm{vmr}}{1+\mathrm{vmr}} \times 100 \tag{6}$$

$$ew_{liq(T)} = 6.112 \times e\left(17.62 \times \frac{T - 273.14159}{243.12 + (T - 273.14159)}\right) \quad (7)$$

$$ew_{ice(T)} = 6.112 \times e\left(22.5 \times 1 - \frac{273.14159}{T}\right) \quad (8)$$

$$W = \frac{M_w}{M_d} \mathrm{x} \frac{RH}{100} \mathrm{x} \frac{ew_{(T)}}{\left(P - \frac{RH}{100} \mathrm{x} ew_{(T)}\right)} \mathrm{x}1000 \quad (9)$$

$$vmr = \frac{M_d}{M_w \mathrm{x} W \mathrm{x}1000} \quad (10)$$

Here RH^i represents the relative humidity with respect to ice, whereas RH^l represents the relative humidity with respect to liquid.

P: Pressure in mbar

vmr: volume mixing ratio in parts per million

T: Temperature in K

$ew_{liq(T)}$: saturation partial pressure over liquid water at given temperature

$ew_{ice(T)}$: saturation partial pressure over ice at given temperature

$M_w = 18.0160$ (molecular weight of water)

$M_d = 43.3400$ (molecular weight of dry air on Mars)

W = water mass mixing ratio

3.2. Thermal behaviour with an instrument with internal heating: HABIT for ExoMars

This study investigates the expected thermal distribution when a simplified model of the HabitAbility: Brines, Irradiance and Temperature (HABIT) instrument is placed inside the chamber at Martian conditions [34]. HABIT is one of the two European payloads on the Surface Platform Kazachok that is part of the ExoMars 2022 mission to Mars [34]. HABIT consists of two modules (i) Container unit (CU) and (ii) Electronic unit (EU), the main objective of this instrument is to characterize the habitability and demonstrate the in-situ resource utilization (ISRU) on Mars. The CU unit has six different containers fitted with electrodes in each container. This unit will carry four different deliquescent salts in four different containers and two empty containers will collect airborne dust. These salts are known to exist on the surface of Mars. It has been hypothesized that upon exposure with the small amounts of water contained in the Martian atmosphere, these salts would hydrate or deliquesce allowing for an active present-day atmosphere-regolith interaction. The electronics in the instrument is protected from the extreme temperatures through the heaters in the EU which are activated when the temperature drops below 240 K and is disabled if it raises above 243 K. Additionally, there is a heater on the CU which can be activated upon command to dehydrate the salts and restart the experiment.

In this present study, we model only a simplified version of the CU of HABIT Engineering Model (EM), shown in Fig. 9. This unit is made of aluminium, it has 6 different containers, the container unit measures 150 mm × 63 mm × 43 mm and has an insulating base made of ABS plastic. We shall compare the simulated results with the results obtained in the experiment with the full HABIT instrument (i.e. both EM and CU) [34]. Since we have not included the EU to simplify the complexity of the simulation, we assume here that the heating of the EU is directly applied to the CU (which represents 40% of the total mass of HABIT instrument).

In our simulation, the heater works with a power of 8.8 W which activates when the temperature drops below 240 K and is disabled when temperature reaches 243 K. Along with this, to mimic the real operation, in our simulation we also supply a continuous power of 0.44 W to the CU for the sensors and electronics to function and record the data. This modelled CU is subjected to the Martian night to day simulation as done in the 3.1.2 section to study the thermal distribution of the instrument when placed inside and apply the heating resistance at the nominal night-time temperature and compare it with the experimental data. The initial temperature of the table is set to 200 K and the container unit is set initially to an arbitrary low temperature of 243 K, which is similar to the first registered temperature of the HABIT-CU temperature in our experiment. In the simulation, we observe as time evolves the CU warms up and maintains the temperature above 240 K (this is the requirement for the electronics to operate on Mars) and the trend is similar to the previous experiment (Fig. 10). But we see a thermal offset between the experimental and simulation temperatures of the CU. We hypothesize that this temperature difference is because the CU in the experiment is filled with 6 g of salts. When the upper layers of these salts interact with the atmospheric moisture there is an exothermic reaction that produces heat.

Indeed, previous research on the equivalent power produced by the hydration or deliquescence of certain salts has demonstrated that, for instance, the hydration of K_2CO_3 and $MgCl_2{\cdot}2H_2O$ at 7.5 mbar produces a peak power of 0.31 W/g at 32 °C and 0.3 W/g at 42 °C respectively [35]. Similarly, the hydration of pure $CaCl_2$ reaches an average power of 0.5 W/g at 80 °C [36]. In our study, we can qualitatively match the thermal behaviour if we increase the continuous power supply to the CU from 0.44 W to 1.5 W (arbitrary value). We conclude that the extra 1.06 W power can be produced by the hydration and deliquescence of the upper layers of the 6 g of the four deliquescent salts in the HABIT container. An example of such exothermicity is clearly observed in the experimental measurements shown in Fig. 10, as a sudden rise in temperature at 370 min. Although this simulation is not fully representative of the experiment as we have not modelled the EU and not included the

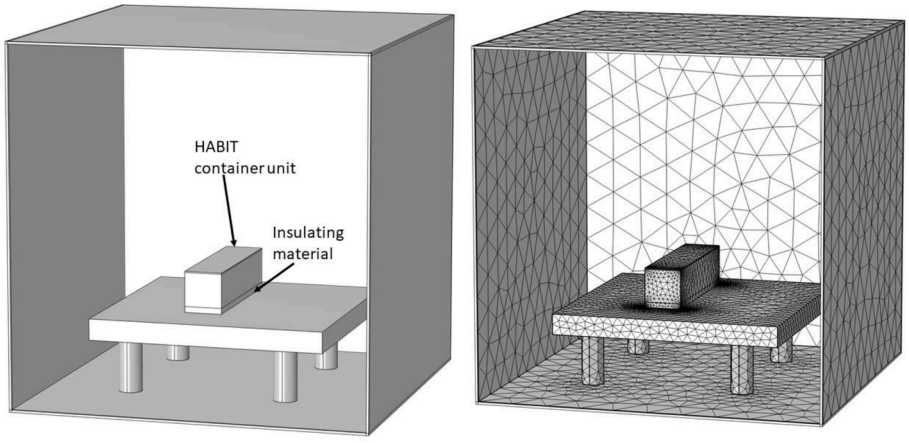

Fig. 9. Schematic and meshed view of the chamber with the HABIT container unit placed inside.

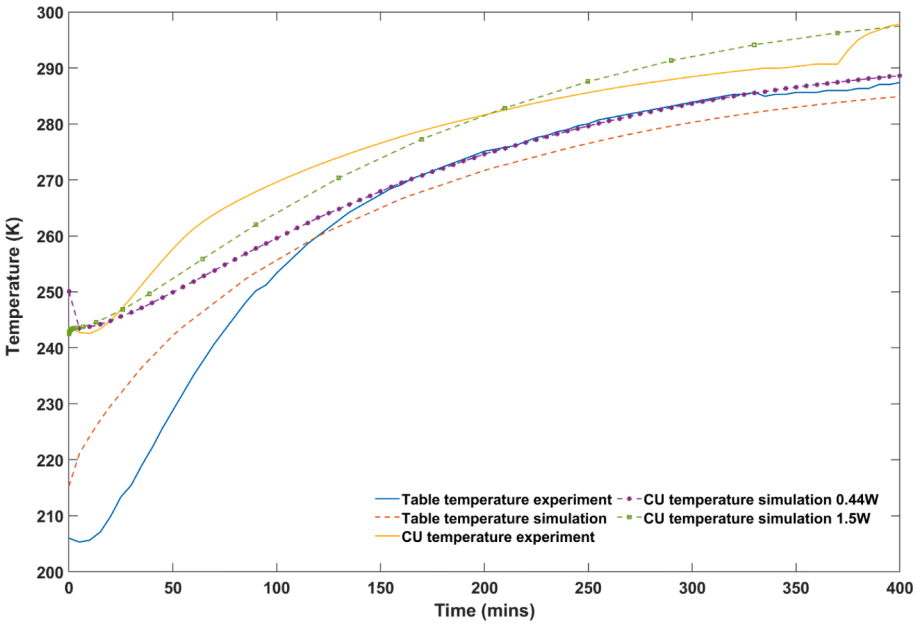

Fig. 10. Comparison of the time evolution under Martian conditions of the table temperature (Tg) and container unit temperature (Tcu) from COMSOL simulation and experimental measurements. The CU temperature is simulated for two different continuous power levels of 0.44 W and 1.5 W to compare with the experimental data.

salts inside and the CU, this simplified study can help us understand the heat exchange processes and be used to interpret qualitatively the calorimetric studies of experiments under Martian conditions with water hydration. In the simulation, after 400 min the CU with 0.44 W and the table temperature equilibrates around 289 K and 285 K, respectively.

Fig. 11 shows the overall thermal distribution inside the chamber at different time intervals where we can observe how the table and CU equilibrates at the end of the simulation. As the water vapor is not simulated in this model, we use this simulation of HABIT CU to calculate numerically using equations 6–10. At each grid point using the temperature and pressure from the simulation and the one-point air relative humidity from the experiment. Fig. 12 shows the 2D cross section and evolution of relative humidity inside the chamber at different intervals of time. We observe that water first condenses on the table, at 200 K, where the relative humidity is saturated, and frost formations starts. As the temperature increases the water redistributes and the full chamber will be almost saturated by the end of 400 min. The time evolution of the relative humidity of the table in the simulation shows saturation at the

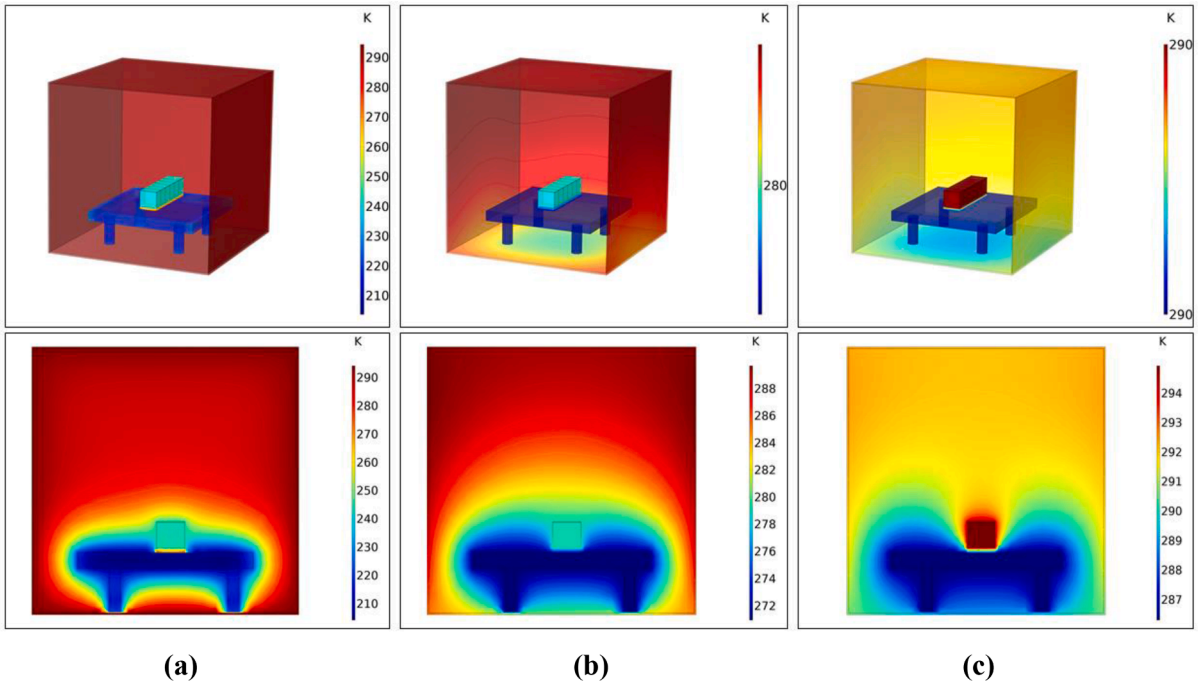

Fig. 11. Time evolution of the temperature profile under Martian conditions with container unit of HABIT inside the chamber (Top) 3D model of the chamber (Bottom) 2D cross-section view model of the chamber (a) shows the overview of the temperature distribution inside the chamber at 0 min with the working plate close to 200 K (b) temperature distribution inside the chamber at 200 min (c) temperature distribution inside the chamber at 400 min.

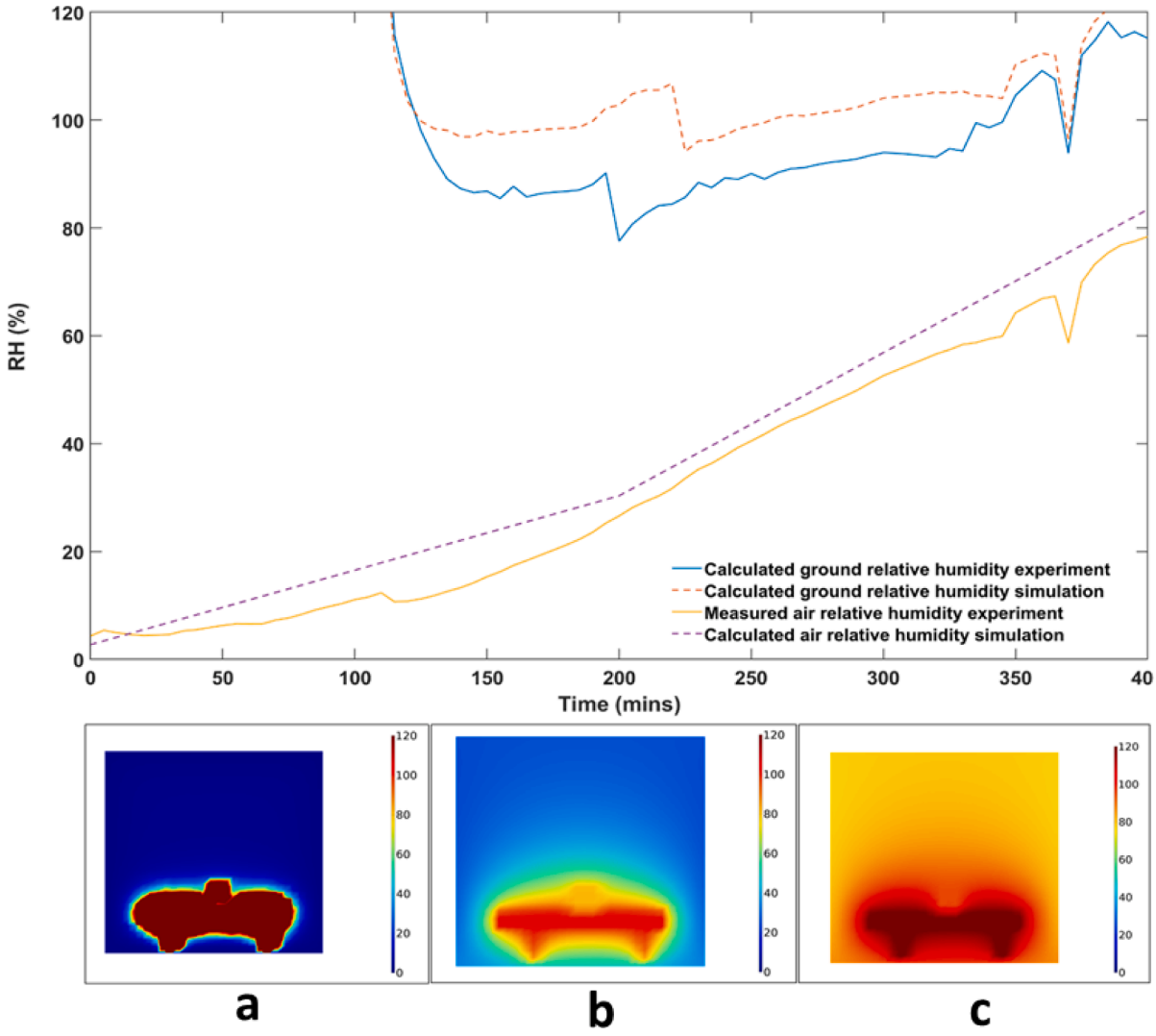

Fig. 12. (Above) Calculated relative humidity of the ground (RHg) and air (RHa) from the simulation and the experiment. (Below) 2D cross-section of the time evolution of the relative humidity RH under Martian conditions inside the chamber with the CU placed on the table in percentage (%). (left) shows the overview of the relative humidity inside the chamber at 0 min which shows over saturation at the working table which for these conditions shall lead to frost formation (middle) RH at 200 min, at this RH frost is no longer stable and should sublimate or be transiently stable as liquid, (right) RH at 400 min. The chamber has reached an almost uniform level of 80–90% RHa.

beginning, similar to the table refrigerated at the start and covered with frost in the experiment. As the time evolves the temperature increases and the water droplets start to appear on the table, later on these droplets release slowly back to the atmosphere as water vapor, allowing for the RHa to increase which is in turn captured by the salts in the container.

3.3. Qualification conditions at vacuum

In the case of heating in vacuum the chamber has an option to be fitted with an external heating jacket of 700 W input power made of glass wool with a thickness of 15 mm. The aim of this qualification test is to perform Thermal Vacuum Tests (TVT), or outgassing studies or to apply sterilization through the Dry Heat Microbial reduction (DHMR) procedures. These tests play a significant role in validating the integrity and thermal efficiency of the components. High vacuum, radiation exposure and changing temperatures are the predominant atmospheric conditions in space. Thus, any component or scientific instrument must be checked to demonstrate that it survives through this thermal dynamic phase before launch. Before subjecting the chamber to such high levels of temperature in vacuum and to understand the thermal distribution inside along with time to reach 420 K (limit to perform TVT and DHMR test) we use this COMSOL model. The external domain of the model (Fig. 2) is applied as the heat source with 700 W power and the fluid domain inside the chamber is Earth air with a pressure of 10^{-3} mbar.

In this section we simulate the expected behaviour of the chamber at the upper temperature limit of the chamber by heating the external walls at vacuum conditions using a heating jacket. For this purpose we use the model as in the previous section, in addition we apply a heating jacket with a input power of 700 W on the outer walls and instead of CO_2 gas we replace it with air at 10^{-3} mbar (vacuum conditions). The required computational time of the 3D model for each study case is around 2 h. We observe in Fig. 13 the temperature profile of the chamber, at the start of the experiment we see that the chamber is at ambient temperature conditions at 295 K. As the time increases the external walls where the jacket is fitted, heat up and the temperature dissipates inwards to the table. We observe that it takes around 150 min to heat the working table to 420 K. It is in this plate where instruments would be mounted and if we consider the mass of the instrument, this upper temperature limit will probably be reduced once the instrumentation is set inside the chamber. This information is essential to plan the duration of experiments and know in advance the thermal stress that the hardware or

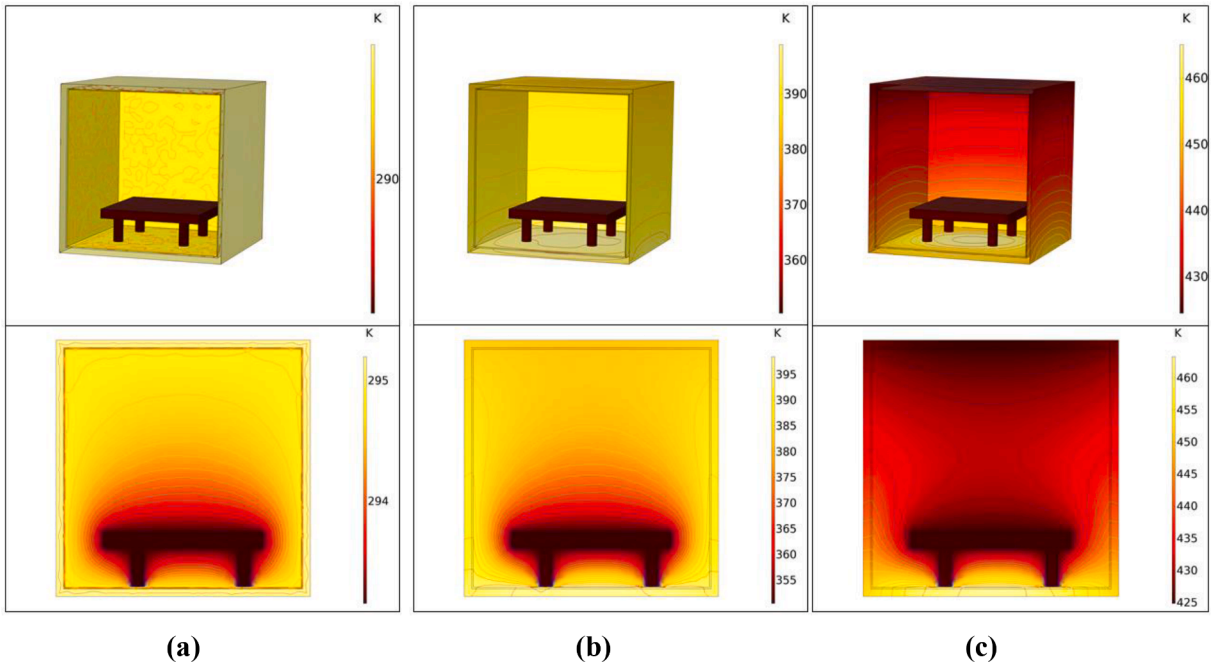

Fig. 13. Time evolution of the temperature profile inside the chamber under vacuum conditions (Top) 3D view of the chamber and (Bottom) 2D cross-section when the heating jacket is operating at the external boundaries (a) shows the overview of the temperature distribution of the chamber at 0 min at ambient 295 K, (b) at 75 min, (c) at 150 min as the temperature of the table reaches 420 K.

materials will experience. In particular, at the latest stages, the table (and any element mounted on it) is heated at a rate of 3 K/min. We see the time evolution of temperature in Fig. 14 of the working table temperature and air temperature in 3D model.

Fig. 15 shows that heat transfer mode is dominated by conduction as the external walls of the chamber are heated up. The maximum intensity of the heat flux through conduction is around 2300 W/m^2 at the walls where the heating jacket is in close contact. This heating jacket can provide a maximum heat flux up to 6500 W/m^2. The blackbody radiation intensity (Fig. 16) heat transfer mode is the next dominant source which is maximum at 800 W/m^2 at the bottom of the chamber as the walls slowly radiates the heat inwards into the chamber. The convective mode of heat transfer is minimal as the air inside is in vacuum and does not affect the model in any significant way.

5. Conclusions and future work

We have performed 3D model thermal simulation studies of the SpaceQ experimental facility using COMSOL to model the time evolution of temperature distribution within the chamber during its

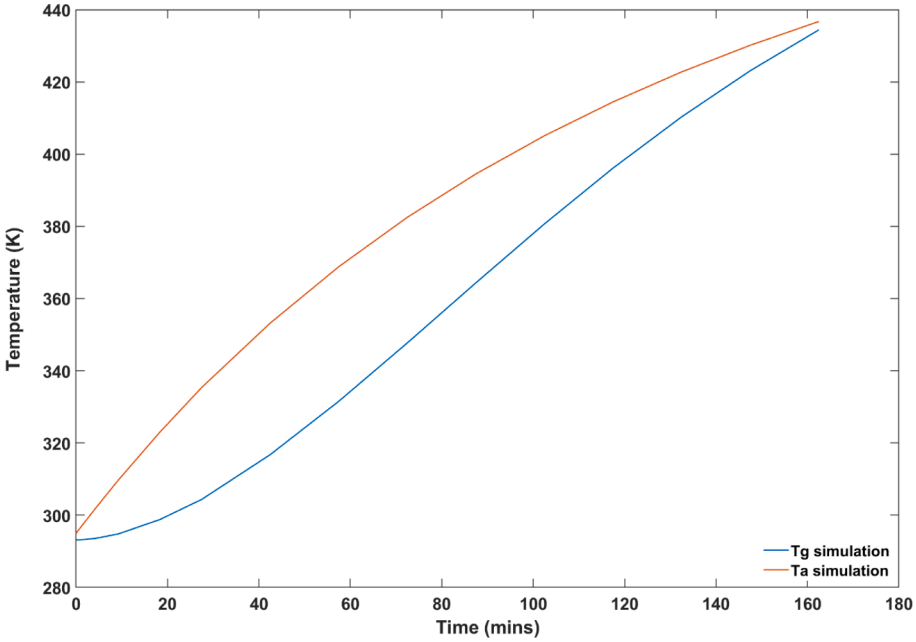

Fig. 14. Comparison of the time evolution of the table temperature (Tg) and air temperature (Ta) from simulation under vacuum condition with an external heating jacket.

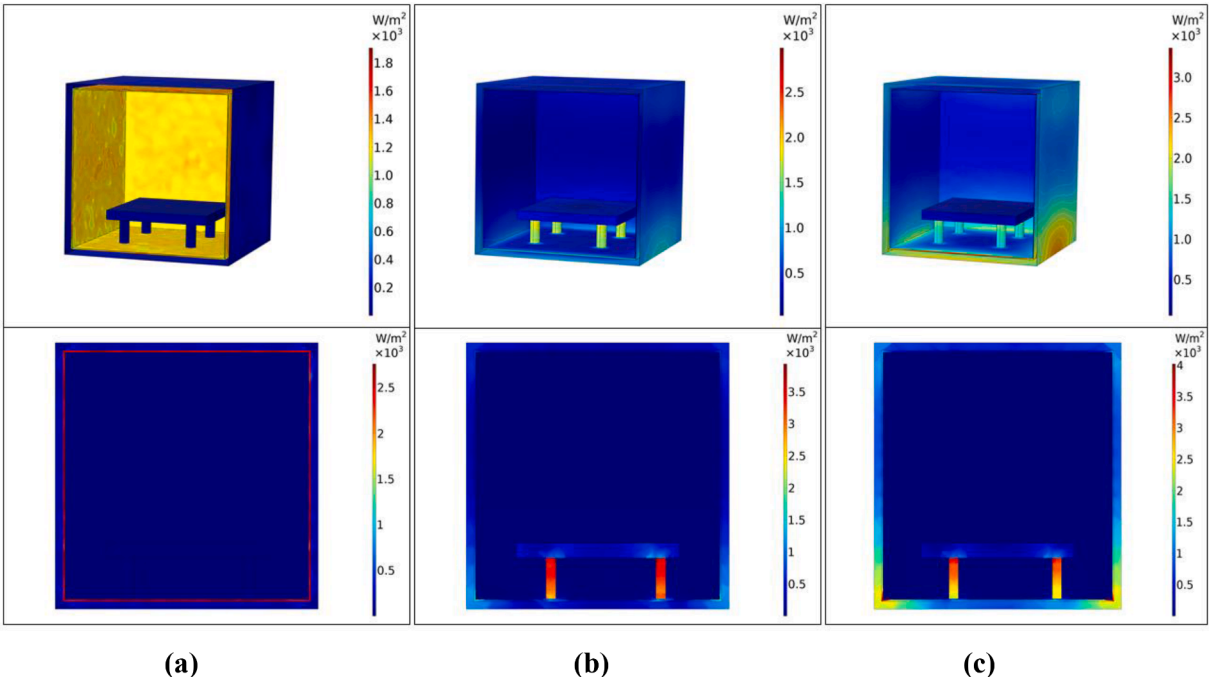

Fig. 15. Conductive heat flux magnitude inside the chamber under vacuum condition with an external heating jacket (Top) 3D view of the chamber and (Bottom) 2D cross-section when the heating jacket is operating at the external boundaries (a) shows the overview of the conductive heat flux inside the chamber at 0 min (b) conductive heat flux inside the chamber at 75 min (c) conductive heat flux inside the chamber at 150 min.

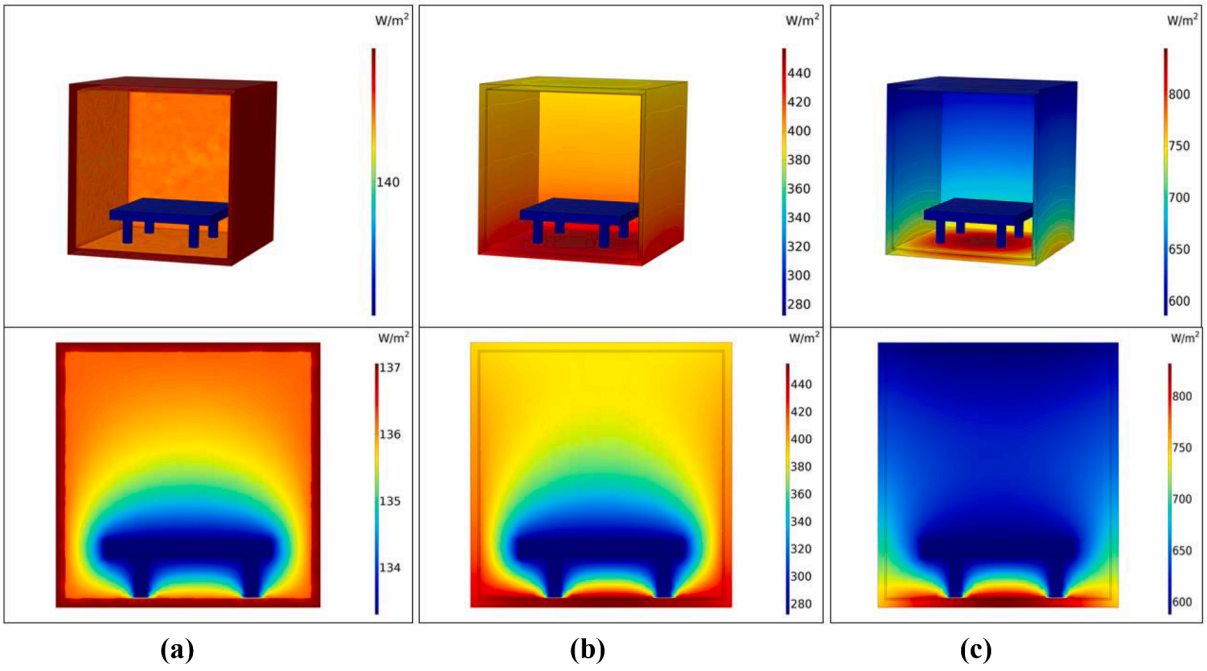

Fig. 16. Blackbody radiation intensity inside the chamber under vacuum condition with an external heating jacket (Top) 3D view of the chamber and (Bottom) 2D cross-section when the heating jacket is operating at the external boundaries (a) shows the overview of the radiation intensity inside the chamber at 0 min (b) radiation intensity inside the chamber at 75 min (c) radiation intensity inside the chamber at 150 min.

operation. Accurate knowledge of the actual temperature, its evolution and gradients, and the heat-flux sources and sinks are critical to design and upgrade the chambers, to plan experiments and to interpret observations. This study gives a full representation of the system and compares the results with our experimental data. We simulate some of the different experimental conditions which are routinely tested inside the chamber (i) near surface water cycle at Martian temperature and pressure (ii) thermal behaviour when HABIT is operated under Martian temperature, pressure and water content conditions (iii) heating in vacuum for qualification or sterilization tests.

In the first condition, we have modelled and simulated the near surface water cycle with Martian temperature and pressure inside the chamber. This study condition was to create a plausible night-day transition as on the near surface of Mars. We have validated the

simulation results with the experimental data by comparing the thermal control points of the table and air temperature inside the chamber which shows good agreement on the equilibration time scales and thermal gradients. This model is further validated by the extrapolating the one-point relative humidity of the experimental data to each grid points in the simulation using temperature and pressure values. This calculated relative humidity for simulation model shows correlation with the appearance of frost and liquid water droplets as observed in the studies associated with the Martian water cycle experiment. We have also modelled a simplified version of the hydration tests of the ExoMars HABIT (HabitAbility: Brine Irradiation and Temperature) instrument container unit (CU). This model shows that, in addition to the continuous effect of the externally applied electronics power, there is an extra internal heating source of about 1 W which can be attributed to the hydration and deliquescence of the salts in the CU when exposed to Martian conditions and contact with atmospheric moisture.

Our third study case simulates the heating of the chamber walls to evaluate the thermal hotspots and the time needed for the chamber to reach the targeted upper limit temperature (420 K) of the qualification tests under vacuum. This study shows that the chamber requires approximately 2.5 h to reach 420 K without any instruments placed inside for testing. If we consider the mass of the instrument the time required will probably increase, this is an important information to plan the duration of experiments. Further analysis of the model shows the conductive heat flux is predominantly observed at the external walls as it heats up and then at the bottom wall of the chamber close to the working table.

The simulation study that we have presented may be used by engineers and scientists to simulate their own space simulating facilities. Future studies will focus on simulations including the two units of HABIT inside the chamber to compare with actual observations during operations on Mars. In the future, we will include other materials like regolith emulant, solid rock cores and dust to understand the thermal behaviour of these materials exposed to Martian surface environmental conditions. Also, an additional temperature sensor will be added in the future experiments, in particular on the outer shell, to compare with the simulations and further characterise these strong thermal gradients.

CRediT authorship contribution statement

Abhilash Vakkada Ramachandran: Conceptualization, Methodology, Software, Data curation, Validation, Investigation, Writing – original draft. **María-Paz Zorzano:** Conceptualization, Methodology, Validation, Supervision, Writing – review & editing. **Javier Martín-Torres:** Validation, Supervision, Writing – review & editing.

Declaration of Competing Interest

The authors declare that they have no known competing financial interests or personal relationships that could have appeared to influence the work reported in this paper.

Acknowledgements

The authors would like to acknowledge COMSOL® advisors for their support and Dr. Miracle Israel Nazarious for his valuable inputs on the HABIT data. MPZ acknowledges the partial support of the Agencia Estatal de Investigación Project No. MDM-2017-0737 Unidad de Excelencia “María de Maeztu” – Centro de Astrobiología (CSIC-INTA), and the Ministerio de Ciencia e Innovación (ref. PID2019-104205GB-C21). The Kempe Foundation funded the design and fabrication of the SpaceQ chamber. A.V.R. and J.M.T. acknowledge support from the Wallenberg Foundation.

References

[1] A.I. Zhukova, I.I. Kondratyev, On artificial Martian conditions reproduced for microbiological research, Life Sci. Space Res. 3 (1965) 120–126.
[2] J.M. Sobrado, J. Martín-Soler, J.A. Martín-Gago, Mimicking Mars: A vacuum simulation chamber for testing environmental instrumentation for Mars exploration, Rev. Sci. Instrum. 85 (3) (2014) 035111, https://doi.org/10.1063/1.4868592.
[3] E. Mateo-Martí, O. Prieto-Ballesteros, J.M. Sobrado, J. Gómez-Elvira, J.A. Martín-Gago, A chamber for studying planetary environments and its applications to astrobiology, J Ǵ 17 (8) (2006) 2274–2280, https://doi.org/10.1088/0957-0233/17/8/031.
[4] L.L. Jensen, J. Merrison, A.A. Hansen, K.A. Mikkelsen, T. Kristoffersen, P. Nørnberg, B.A. Lomstein, K. Finster, A Facility for Long-Term Mars Simulation Experiments : The Mars Environmental Simulation Chamber (MESCH), 8 (2008). https://doi.org/10.1089/ast.2006.0092.
[5] M. Patel, K. Miljkovic, T. Ringrose, M. Leese, The Hypervelocity Impact Facility and Environmental Simulation at the Open University, (2010).
[6] European Cooperation For Space Standardization, ECSS-Q-ST-70-02C: Thermal vacuum outgassing test for the screening of space materials, (2008).
[7] S. Division, Space product assurance Dry heat bioburden reduction for, (2013).
[8] N.I. Kömle, P. Tiefenbacher, P. Weiss, A. Bendiukova, Melting probes revisited – Ice penetration experiments under Mars surface pressure conditions, icarus. 308 (2018) 117–127, https://doi.org/10.17632/hnyrvgd6zy.1.
[9] F.J. Martín-Torres, M.-P. Zorzano, P. Valentín-Serrano, A.-M. Harri, M. Genzer, O. Kemppinen, E.G. Rivera-Valentin, I. Jun, J. Wray, M. Bo Madsen, W. Goetz, A. S. McEwen, C. Hardgrove, N. Renno, V.F. Chevrier, M. Mischna, R. Navarro-González, J. Martínez-Frías, P. Conrad, T. McConnochie, C. Cockell, G. Berger, A. R. Vasavada, D. Sumner, D. Vaniman, Transient liquid water and water activity at Gale crater on Mars, Nat. Geosci. 8 (5) (2015) 357–361, https://doi.org/10.1038/ngeo2412.
[10] S. Byrne, A.P. Ingersoll, A Sublimation Model for Martian South Polar Ice Features, Science (80-.). 299 (2003) 1051 LP – 1053. https://doi.org/10.1126/science.1080148.
[11] G.M. Martínez, C.N. Newman, A. De Vicente-Retortillo, E. Fischer, N.O. Renno, M. I. Richardson, A.G. Fairén, M. Genzer, S.D. Guzewich, R.M. Haberle, A.-M. Harri, O. Kemppinen, M.T. Lemmon, M.D. Smith, M. de la Torre-Juárez, A.R. Vasavada, The Modern Near-Surface Martian Climate: A Review of In-situ Meteorological Data from Viking to Curiosity, Space Sci. Rev. 212 (1-2) (2017) 295–338, https://doi.org/10.1007/s11214-017-0360-x.
[12] L. Zhang, G. Liu, W. Leng, A.S. Method, Development of the Simulation & Experiment System for Martian Atmosphere Simulation Environment Box 159 (2018) 60–63.
[13] A.I. Alsabery, M.A. Sheremet, A.J. Chamkha, I. Hashim, Energy transport of two-phase nanofluid approach inside a three-dimensional lid-driven cubic cavity containing solid cylinder and heat source, Chem. Eng. Process. – Process Intensif. 154 (2020), 108010, https://doi.org/10.1016/j.cep.2020.108010.
[14] Y. Sun, G. Lin, X. Bu, L. Bai, C. Xiao, D. Wen, A numerical study of fluid flow and heat transfer in carbon dioxide enclosures on mars, Energies. 11 (2018) 1–19, https://doi.org/10.3390/en11040756.
[15] A. Mochida, K. Kudo, Y. Mizutani, M. Hattori, Y. Nakamura, Transient heat transfer analysis in vacuum furnaces heated by radiant tube burners, Energy Convers. Manag. 38 (1997) 1169–1176, https://doi.org/10.1016/S0196-8904(96)00146-X.
[16] F. Hötte, M.C. Haupt, Transient 3D conjugate heat transfer simulation of a rectangular GOX – GCH 4 rocket combustion chamber and validation, Aerosp. Sci. Technol. 105 (2020) 106043, https://doi.org/10.1016/j.ast.2020.106043.
[17] A. Soria-Salinas M.-P. Zorzano J. Martín-Torres J. Sánchez-García-Casarrubios J.-L. Pérez-Díaz A. Vakkada-Ramachandran A Xenon Mass Gauging through Heat Transfer Modeling for Electric Propulsion Thrusters Int. J. Mech. Aerospace, Ind. Mechatron. Manuf. Eng. 11 2017 94 105 http://waset.org/Publications?p=121.
[18] G.A. Harris, F.M. Fernández, Simulations and experimental investigation of atmospheric transport in an ambient metastable-induced chemical ionization source, Anal. Chem. 81 (1) (2009) 322–329, https://doi.org/10.1021/ac802117u.
[19] A.A. Bhat, D. Sujish, S. Agarwal, B. Muralidharan, G. Padmakumar, K.K. Rajan, Electromagnetic and Thermal Modeling of Vacuum Distillation Furnace, 2013 COMSOL Conf. Bangalore. (2013) 1–5.
[20] Iván D. Palacio-Caro, Pedro N. Alvarado-Torres, Luis F. Cardona-Sepúlveda, Numerical simulation of the flow and heat transfer in an electric steel tempering furnace, Energies. 13 (14) (2020) 3655, https://doi.org/10.3390/en13143655.
[21] Matthew A. Siegler, Suzanne E. Smrekar, Matthias Grott, Sylvain Piqueux, Nils Mueller, Jean-Pierre Williams, Ana-Catalina Plesa, Tilman Spohn, The InSight Mars Lander and Its Effect on the Subsurface Thermal Environment, Space Sci. Rev. 211 (1-4) (2017) 259–275, https://doi.org/10.1007/s11214-017-0331-2.
[22] H. Behi, M. Behi, D. Karimi, J. Jaguemont, M. Ghanbarpour, M. Behnia, M. Berecibar, J. Van Mierlo, Heat pipe air-cooled thermal management system for lithium-ion batteries: High power applications, Appl. Therm. Eng. 183 (2021), 116240, https://doi.org/10.1016/j.applthermaleng.2020.116240.
[23] E. Díez-Jiménez, R. Alcover-Sánchez, E. Pereira, M.J. Gómez García, P.M. Vián, Design and test of cryogenic cold plate for thermal-vacuum testing of space components, Energies. 14 (2019) 1–22, https://doi.org/10.3390/en12152991.
[24] S. Wang, K. Li, Y. Tian, J. Wang, Y. Wu, S. Ji, An experimental and numerical examination on the thermal inertia of a cylindrical lithium-ion power battery, Appl. Therm. Eng. 154 (2019) 676–685, https://doi.org/10.1016/j.applthermaleng.2019.03.141.
[25] X. Yang, G. Lv, W. Ma, H. Xue, D. Chen, The effect of radiative heat transfer characteristics on vacuum directional solidification process of multicrystalline

silicon in the vertical Bridgman system, Appl. Therm. Eng. 93 (2016) 731–741, https://doi.org/10.1016/j.applthermaleng.2015.10.073.
[26] H. Charvátová, A. Procházka, M. Zálešák, Computer simulation of temperature distribution during cooling of the thermally insulated room, Energies. 11 (2018) 1–16, https://doi.org/10.3390/en11113205.
[27] A. Vakkada Ramachandran, M.I. Nazarious, T. Mathanlal, M.-P. Zorzano, J. Martín-Torres, Space Environmental Chamber for Planetary Studies, Sensors. 20 (2020) 3996, https://doi.org/10.3390/s20143996.
[28] Miracle Israel Nazarious, Abhilash Vakkada Ramachandran, Maria-Paz Zorzano, Javier Martin-Torres, AU – Martin-Torres, Measuring Electrical Conductivity to Study the Formation of Brines Under Martian Conditions, JoVE. (173) (2021), https://doi.org/10.3791/61217.
[29] M. Schoenenberger, F.M. Cheatwood, P. Desai, Static Aerodynamics of the Mars Exploration Rover Entry Capsule, in: 43rd AIAA Aerosp. Sci. Meet. Exhib., American Institute of Aeronautics and Astronautics, 2005. https://doi.org/doi:10.2514/6.2005-56.
[30] D.G. Murri, Simulation Framework for Rapid Entry, Descent, and Landing (EDL), Analysis. 1 (2010).
[31] Á. Soria-Salinas, M.-P. Zorzano, R. Mantas-Nakhai, J. Martín-Torres, Wind retrieval from temperature measurements from the Rover Environmental Monitoring Station/Mars Science Laboratory, Icarus. 346 (2020), 113785, https://doi.org/10.1016/j.icarus.2020.113785.
[32] A.F. Ismail, K.C. Khulbe, T. Matsuura, Gas separation membranes, Switz. Springer. 10 (2015) 973–978.
[33] Abhilash Vakkada Ramachandran, María-Paz Zorzano, Javier Martín-Torres, Experimental Investigation of the Atmosphere-Regolith Water Cycle on Present-Day Mars, Sensors. 21 (21) (2021) 7421, https://doi.org/10.3390/s21217421.
[34] J. Martín-Torres, M.-P. Zorzano, Á. Soria-Salinas, M.I. Nazarious, S. Konatham, T. Mathanlal, A.V. Ramachandran, J.-A. Ramírez-Luque, R. Mantas-Nakhai, The HABIT (HabitAbility: Brine Irradiation and Temperature) environmental instrument for the ExoMars 2022 Surface Platform, Planet. Space Sci. 190 (2020), 104968, https://doi.org/10.1016/j.pss.2020.104968.
[35] L.C. Sögütoglu, P.A.J. Donkers, H.R. Fischer, H.P. Huinink, O.C.G. Adan, In-depth investigation of thermochemical performance in a heat battery: Cyclic analysis of K2CO3, MgCl2 and Na2S, Appl. Energy. 215 (2018) 159–173, https://doi.org/10.1016/j.apenergy.2018.01.083.
[36] D.P.A. J., A.O.C. G., S.D.M. J., Hydration/Dehydration Processes in Stabilized $CaCl_2$, Poromechanics VI. (2021) 656–663. https://doi.org/doi:10.1061/9780784480779.081.